UCRL-JRNL-407256

LAWRENCE LIVERMORE NATIONAL LABORATORY

Single Crystal Growth and Formation of Defects in Deuterium-Tritium Ice Layers for Inertial Confinement Fusion

A. A. Chernov, B. J. Kozioziemski, J. A. Koch, L. J. Atherton, M. A. Johnson, A. V. Hamza, S. O. Kucheyev, J. B. Lugten, E. A. Mapoles, J. D. Moody, J. D.Salmonson, J. D. Sater

September 15, 2008

Applied Physics Letters

This document was prepared as an account of work sponsored by an agency of the United States government. Neither the United States government nor Lawrence Livermore National Security, LLC, nor any of their employees makes any warranty, expressed or implied, or assumes any legal liability or responsibility for the accuracy, completeness, or usefulness of any information, apparatus, product, or process disclosed, or represents that its use would not infringe privately owned rights. Reference herein to any specific commercial product, process, or service by trade name, trademark, manufacturer, or otherwise does not necessarily constitute or imply its endorsement, recommendation, or favoring by the United States government or Lawrence Livermore National Security, LLC. The views and opinions of authors expressed herein do not necessarily state or reflect those of the United States government or Lawrence Livermore National Security, LLC, and shall not be used for advertising or product endorsement purposes.

Single Crystal Growth and Formation of Defects in Deuterium-Tritium Ice Layers for Inertial Confinement Fusion

A. A. Chernov, B. J. Kozioziemski, J. A. Koch, L. J. Atherton, M. A. Johnson, A.V. Hamza, S. O. Kucheyev, J. B. Lugten, E. A. Mapoles, J. D. Moody, J. D. Salmonson, J. D. Sater

Lawrence Livermore National Laboratory, 7000 East Avenue Livermore CA 94550

ABSTRACT

We identify vapor-etched grain boundary grooves on the solid-vapor interface as the main source of surface roughness in the Deuterium-Tritium (D-T) fuel layers which are solidified and then cooled. Current inertial confinement fusion target designs impose stringent limits to the cross sectional area and total volume of these grooves. Formation of these grain boundaries occurs over timescales of hours as the dislocation network anneals, and is inevitable in a plastically deformed material. Therefore, either cooling on a much shorter time scale or a technique that requires no cooling after solidification should be used to minimize the fuel layer surface roughness.

Starting in 2010, experiments at the National Ignition Facility (NIF) will attempt to achieve fusion ignition of the nuclear reaction D + T = α(3.5 MeV) + n(14.1 MeV) by imploding a thin shell of frozen D-T fuel. This fuel is a solid spherical layer ~ 100 μm thick covering the internal surface of a hollow 2 mm-diameter polymer or beryllium spherical shell with a 40 - 150 μm-thick wall. The fuel is compressed adiabatically by the spherically-imploding laser light converted to x-rays to obtain the final temperatures and densities required to achieve nuclear fusion. Minimizing the initial equilibrium D-T vapor pressure inside the fuel target increases the implosion velocity and hence the compression. The current ignition target design sets the vapor pressure such that the solid D-T temperature is 1.5 K below its triple-point temperature of 19.79 K. Furthermore, the solid D-T layer must be very uniform and smooth to minimize the hydrodynamic instabilities that arise during compression. Producing D-T layers that are sufficiently smooth remains a significant challenge.

In earlier work, hydrogen molecules were pressed to diffuse through the shell at high temperature and then frozen to either crystalline D-T [1,2] or probably amorphous H_2 layers [3]. However, major defects appeared during the post-freeze cooling. Here we analyze crystallization process and the origin and nature of the defects.

Experimental setup

The capsule is suspended by a 30 μm diameter glass fill-tube at the center of a 25 mm diameter cavity machined into an aluminum cube. The cube is mounted on a liquid-helium cooled flow cryostat and controlled to ±2 mK. The cavity is filled with 1-2 torr of ^{4}He gas to conductively cool the capsule. The fill tube is used to deliver the molar 0.5DT

LLNL-JRNL-407256

– $0.25D_2$ – $0.25T_2$ mixture into the capsule. The target is visualized by transmission optical microscopy and by phase contrast refraction x-ray imaging [4,5] .

Crystallization

D-T is liquid at $T > T_m$ =19.79K (triple point) and adheres strongly to the substrate, forming an extended meniscus on the bottom (Fig. 1a). Frozen slowly, at cooling rate of 10^{-5} – 10^{-6} K/s, many layers form single crystals with very few defects observable in either the x-ray or visible light images. These layers tend to form reproducibly, presumably from a seed near or in the fill-tube. The crystal emerges from the fill tube (Fig. 1b) as a narrow rod (tens of microns wide in cross section) and grows rapidly along its major axis. The two ends of the rod meet one another in the bottom melt region, forming a closed equatorial belt. Then the belt expands in width (Fig. 1c), eventually covering the whole inner surface of the capsule closing near two poles. Sometimes the growth front leaves behind circular features near the poles, the "arctic circles", (arrow in Fig. 2a) that persist. The symmetry of defects discussed below, strongly suggests that the layer forms as HCP single crystal [6]. Very fast cooling of the vapor and melt often results in a layer with many defects, which suggests a polycrystalline layer.

We interpret the processes as follows. Nanocrystalites of D-T may remain within cavities in the filling tube wall while all the D-T in the shell is liquid – analogous to conventional crystals [7]. The closest packed basal plane (0001) is molecularly smooth. Its growth occurs layer-by-layer. Conversely, the *a*-interfaces normal to the basal plane and parallel to c-axis are disordered by thermal fluctuations to be molecularly rough. These *a*-surfaces grow much faster, molecule-by-molecule [7]. The crystal with the fastest growing direction along the tube axis emerges and serves as the reproducible seed for the D-T layer. Its basal plane may be nearly parallel to the tube and thus normal to the capsule wall nearby. The rod-shaped belt expands rapidly along the equator because its two end *a*-type rough interfaces are in contact with the cold wall, thus allowing rapid latent heat removal. The belt interface looking towards the center of the sphere is also rough. However, it is heated by the tritium β-decay by $\sim \lambda q h^2/4\kappa\omega$ = 1mK where h = 100 μm is the distance from the wall (Suppl. 1,2). The decay frequency $\lambda = 1.78\times10^{-9}$ 1/s, the β-heat per decay $q = 9.11\times10^{-9}$ erg, the specific molecular volume $\omega = 3.3\times10^{-23}$ cm^3, and the thermal conductivity of D-T $\kappa = 3.5\times10^4$erg/cm/s/K [8]. This temperature rise is close to the supercooling driving the growth, and thus limits the maximum layer thickness h. The same mechanism makes the layer thickness constant over the whole surface in $2H_s/\lambda q \sim 2$ hours, where $H_s = 2.6\times10^{-14}$ erg is the sublimation heat [9]. The kinetic coefficients [7], β, for D-T crystal growth from vapor and melt are estimated to be 6.6 cm/s/K and 1.7×10^3cm/s/K, respectively (Suppl. 2). Then the ratio of the molecular incorporation rate to the heat transport rate [7] is $\beta h H_s/\kappa\omega \sim 5.10^3 >> 1$, so that the growth is limited by the heat transport rather than by interface kinetics. This conclusion is valid also for the slower smooth basal plane.

Cooling defects

Layers formed as described above and kept at $\Delta T <\sim 0.2$ K below the melting temperature may have very few visible defects, except for "arctic circles" (Fig.2a). Cooling these

layers by $\Delta T \sim 1K$ below T_m first induces latitude circles (Fig. 2b), which are estimated from optical imaging to be inner surface perturbations with ~ 0.1 μm amplitude. These circles are observed after several seconds during fast cooling at $(1 - 3)x10^{-2}$ K/s down to (T_m – 1.5K). Annealing at this temperature induces meridian segments several to tens of microns wide (Fig. 2b). These segments often experience a short meridional shift if they come across latitudinal circles (Fig. 2b). Over tens of minutes to hours, ripening of the meridian segments occurs, where shorter segments disappear while the longer meridians coalesce to the twelve- or six-fold symmetry crosses showing strong contrast (Fig 2c). The twelve-fold symmetry (Fig. 2d) appears at middle latitudes while the six-fold symmetry appears nearer to the poles. Phase contrast enhanced x-ray imaging reveals the cusp-like profile of the meridians when they are oriented normal to image plane (limb-on, Fig 3a). The deepest cusps reach ~ 20 μm, the most shallow go below detection limit of ~ 2 μm. Meridians appearing away from the limb are also seen as faint black/white lines (Fig 3a). The optically visible arctic circles are too shallow to be seen with x-ray imaging.

The features described above appear because of differences between the capsule and D-T thermal expansion coefficients, α. For all capsule materials, $\alpha \sim 10^{-5}$ 1/K versus α_a $=1.82x10^{-3}$ 1/K for D_2 along the *a*-directions, i.e. within the c-plane, and $\alpha_c = 1.24x10^{-3}$ 1/K along the c-directions, at 18K [10]. Like all hydrogens, solid D-T seems to adhere to all capsule materials very well: the D-T thermal contraction compresses the shell accordingly. Peeling the ice off the shell was observed by x-ray imaging only once at fast cooling down to T ~ 10K over ~ 10 s. Thus the thermal strain in D-T layer cooled by ΔT =1.5K is ~ $(\alpha_a + \alpha_c)\Delta T/2 \sim 0.2\%$. In accordance with the thermal contraction anisotropy we observed contraction of the cooled capsule in the a-direction by 0.5 μm more than in the c-direction. This ellipticity disappears in about an hour. Free standing cm-size hydrogen samples (D_2, H_2) at T = 14-17K tolerate uniaxial tension strain of up to ~ 20% before they fracture [6]. Similar extreme plasticity is expected for our D-T, especially close to the melting point, $T/T_m \sim 0.9$. During this plastic flow, glide bands and a dislocation network develop, along with flows of vacancies and/or interstitials. Thus the latitudinal circles should be slip bands along the basal planes (0001) in the [2-1-10] direction, the easiest slip system in HCP lattice [11].
At constant or extremely slowly changing temperature, a dislocation network in D-T developed during its plastic flow ripens to minimize the network energy and internal stress. This relaxation creep is assisted by point defects and results in grain boundary formation. Similar to a crystal-melt interface [12], a groove with the cusp-like profile y = y(x) should appear at the line where a grain boundary crosses the crystal-vapor interface. It is this groove that provides the optical (Fig.2) and x-ray (Fig.3a) visible contrast. We choose the y-axis normal to the crystal-vapor interface towards capsule while the x-axis lies within this interface and is normal to the groove. At the cusp line, the interface orientation changes by the angle $\pi - 2\psi_0$, to balance grain boundary energy, γ_{gb}, by the free energies, γ, of two crystal-vapor surfaces. Thus $\sin\psi_0 = \gamma_{gb}/2\gamma$. Evidently, ψ_0 increases with dislocation density in grain boundary or a glide band. Away from the cusp, equilibrium vapor pressure increases due to interface curvature. This increase is compensated by the parabolic ice temperature and thus the vapor pressure decrease towards the ice-capsule interface through which the β-decay heat is released (Suppl.3):

$$(1+p^2)^{-3/2}d^2y/dx^2=(cq\lambda H_s/4\omega^2\kappa\gamma T)y^2\equiv y^2/\lambda^3,\lambda\equiv(4\omega^2\kappa\gamma T/cq\lambda H_s)^{1/3},p\equiv dy/dx \quad (1)$$

The boundary conditions are: $p=0$ far away from the groove, at $y=0$, and $p=p_0=\pm tg\psi_0$ at the cusp line, $x=0$. Approximate integral of eq.(1) gives the half-groove shape *y=y(x)* (Suppl.3):

$$1/\sqrt{y}=1/\sqrt{y_0}+|x|/\sqrt{6}\lambda^{3/2}, \quad (2)$$

where $y_0=y(0)$ is the cusp depth. With the parameters used above and γ = 4 erg/cm^2 [9] in eq.(1), the typical length λ= 30 μm. Fig 3b shows a simulated image with the y(x) functional dependence from eq. (2) for the data in Fig. 3a. Fig. 3c presents the experimental profile obtained from the x-ray phase contrast imaging of the most shallow groove plotted in the $1/\sqrt{y}$ vs $|x|$ coordinates, as in eq.(2). Linearity of the plot provides $\lambda=9.5\mu m$, $y/\lambda=0.23.$, y_0 = 2.1μm. Other 14 grooves analyzed show similar linear dependence with λ scattering between ~ 5 to 13 μm and y_0/λ from ~ 0.2 to ~3. From the first integration of eq.(1), the boundary condition $p=p_0$ at $x=0$ is reduced to $y_0/\lambda=[3(1-1/\sqrt{1+p_0^2})]^{1/3}$. Thus the maximal y_0/λ ratio, $3^{1/3}$ = 1.44, should be reached at $p_0=\infty$. Larger y_0/λ ratios are found for deepest grooves: 1.48, 1.53, 1.58, 2.12, 3.18, 5.16. Most likely, the discrepancy comes, besides experimental error, from inhomogeneous dislocation/stress distribution within the grain since ~1% residual stress results in the ~6.10^{-21}erg shift of crystal chemical potential, comparable with terms in eq.(1) (Suppl.4).

We assume that ice layer is elastically isotropic, much softer than the isotropic capsule, much thinner than internal radius, and no external forces are applied at the layer-vapor interface. Then the thermal shear stress along basal plane *c* in *a*-direction at the latitude θ is σ_{ac} ~ [EΔTsin2θ/2(1-ν^2)][α_a (ν+cos^{2}θ) + $\alpha_c$sin^{2}θ], where E is the Young modulus and ν ~ 0.2 is the Poisson ratio. This shear stress induces basal slip and glide bands with elevated dislocation density and latitudinal grooves. The stress σ_{ac} is maximal at middle latitudes, suggesting maximal dislocation density and thus the density of the grain boundaries there. That may cause six- to twelve-fold symmetry transition in the final groove pattern, Fig. 2c. Typical hour-scale ripening times may be explained on the basis of creep rates [13] to be ~ h^{2}kT/14DEω = 100 minutes at a vacancy diffusivity D = 3x10^{-10} cm^2/s in D-T [14,15] and apparent E = 3x10^8 erg/cm^3 [6] (Suppl. 5) .

"Arctic circle" might be associated with exhaust of material by the expanding of a bit thicker layer and later recondensation. Alternatively, it might come from discontinuous fractionation between D_2, T_2 and D-T at the growing smooth basal plane that relaxed later. No evidence of fractionation is found in DT. However, it happens in the 0.25H_2-0.5HD-025D_2 mixture, since freezing starts at 16.53K ending at 16.10K. [16].

Conclusions. We presented physics behind single crystalline D-T target formation. The major surface defect on the cooled DT-vapor interface are the grain boundary grooves.

They come from ripening of the dislocation network caused by plastic flow caused by ~50 times difference between thermal expansion coefficients of DT and capsule. Latitudinal circles are traces if glide bands. Grain boundaries probably can not be excluded with any approach based on cooling of a single or polycrystalline material. However, cooling within a minute, faster than dislocation ripening, immediately before the implosion may be a solution. The latitudinal glide circles (Fig 2b) still develop, but they are shallow from the perspective of implosion hydrodynamics. The alternative is solidification avoiding cooling stage.

Acknowledgements. Our gratitude goes to Prof. M.E.Glicksman for valuable discussions. This work performed under to auspices of the U.S. Department of Energy by Lawrence Livermore National Laboratory under Contract DE-AC52-07NA27344.

References

1. D.R.Harding, D.D.Meyerhofer, S.J.Loucks, L.D.Lund, R.Janezic, L.M.Elasky, T.H.Hinterman, D.H.Edgell, W.Seka, M.D.Wittman, R.O.Gran, D.Jacobs-Perkins, R.Early, T.Duffy, M.J.Bonino, Physics of Plasmas **13**, 056316 (2006).
2. M. Martin, C. Gauvin, A. Choux, P. Baclet, G. Pascal, Fusion Science and technology **49**, 600-607 (2006).
3. E.Koresheva, I.Osipov, T.Timasheva, L.Yaguzinsky, J.of Physics D:Applied Physics **35,** 825 (2002).
4. D.S.Montgomery et al Scientific Instruments **75,** 3987 (2004).
5. B.J.Kozioziemski, J.A.Koch,A.Barty, H.E.Martz Jr, W-K Lee, K.Fezzaa, J.Appl Phys **97,** 063103 (2005).
6. A.I.Prokhvatilov, Plasticity and Elasticity of Cryocrystals. Handbook. Begel House Inc. NY,Wallingford, UK,2001.
7. A.A.Chernov. Crystal Growth. Modern Crystallography III. Pt 1. Springer Ser Sol.State vol 36. Springer. Berlin 1984.
8. G.W.Collins, P.C.Souers, E.M.Fearon, E.R.Mapoles, R.T.Tsugawa, J.R.Gains, Phys.Rev. **B41,**1816 (1990).
9. P.C.Souers, Hydrogen Properties for Fusion Energy. University of California Press. Berkley, 1986.
10. I.N.Krupski, A.I.Prokhvatilov, G.N.Shcherbakov, Sov.J.Low Temp Phys. **10**,,1 (1984) ; A.I.Prokhvatilov, M.A.Strzhemechnyi, G.N.Shcherbakov, Low Temp. Phys. **20,** 602 (1994).
11. L.A.Shuvalov, A.A.Urusovskaya,I.S.Zheludev, A.V.Zalesskii, S.A.Semiletov, B.N.Grchushnikov, I.G.Chistyakov,S.A.Pikin, Modern Crystallography IV. Physical Properties of Crystals. Springer Ser Sol.State, vol 37 , Springer, Berlin, 1988.
12. R.J.Schaefer, M.E.Glicksman, J.D.Ayers, Phil. Mag. **32,** 725 (1975).
13. M.F.Ashby, Acta Metallurgica **20,** 887 (1972).
14. J.R.Gains, P.A.Fedders, G.W.Collins, J.D.Sater, P.C.Souers, Phys.Rev.**B52,**7243 (1995).
15. C.Ebner, C.C.Sung, Phys Rev **A5,** 2625 (1972).
16. P.W.McKenty, M.D.Wittman, D.R.Harding J.Appl.Phys. **100**, 073302 (2006).

Figure Captions.

Fig. 1. Subsequent stages of crystallization: a. Liquid on the capsule bottom, T > 19.79K; b. Crystalline rod just emerged from the fill tube on the top; c. Belt formed by the rod (Fig.1b) expands towards opposite poles on the left and right; Time is counted from solidification beginning, temperature measured in cryostat.

Fig.2. Cooling induced defects in D-T layer: a Latitudinal "arctic circle" (arrow) is the only visible inhomogeniety in this slowly crystallized layer; the pole, outcrop of the c-axis, is near the circle center; b. Crystallization ended at the poles are on the left and right; latitudinal circles are probably the glide bands along the HCP basal planes; short meridional lines are the vapor-etched grain boundary grooves (cf. cross section in Fig 3a); c.Meridional segments formed by agglomeration of shorter grooves seen in the Fig.3b; Note the six fold symmetry near the pole in the image center in (c) and the twelve fold around the equator in (d). Agglomeration of the grooves visualizes ripening of the dislocation network and corresponding relaxation of the residual stress.

Fig. 3. Groove profile: a. Phase contrast enhanced refraction x-ray images of grooves normal to the limb showing cusp shape; b. The same limb-on images modeled with the functional dependence of eq.(2); c. Groove shape $y = y(x)$ in coordinates of eq.(2) predicting linear dependence of $1/\sqrt{y}$ vs $|x|$, lengths are in microns.

Supplements

1. β-decay heating and limiting growth stage. Growth rate V of a rough surface is linear in supercooling ($T_e - T$) [7]:

$$V = \beta\,(T_e - T). \qquad \text{(S1)}$$

Here β(cm/s.K) is kinetic coefficient that characterizes rate of molecular incorporation into crystal at the phase boundary, T is temperature at the crystal surface, T_e is equilibrium temperature at a given vapor pressure. With the fill tube sealed by crystals, the vapor pressure decreases as crystallization goes. However, full crystallization takes only ~0.1K of temperature drop since at the beginning of freezing major part of DT is in melt. At the triple point, equilibrium vapor pressure over solid, $P_e = 2.08.10^5$erg/cm^3 [9], and changes with temperature as $\partial P_e/\partial T = 7.4.10^4$ erg/cm^3.K. Thus we may ignore the shift of T_e as crystal grows. The temperature T at the growing or retreating DT interface is controlled by its propagation rate, V, β-decay, and heat transport through the DT layer and capsule wall kept at $T = T_0$. For simple estimates, we ignore thermal resistance of the capsule wall as compared to DT layer. Then the temperature T(*r*) within the DT layer

between the spheres $r = r_0 = 1$mm and $r = r_1 = r_0 + h$ obeys the following heat diffusion equation and boundary conditions:

$$(\kappa/r^2)\partial/\partial r(r^2\partial T/\partial r) + q\lambda = 0,\ \ T = T_0 \text{ at } r = r_0,\ \kappa\partial T/\partial r = H_s V/\omega \text{ at } r = r_1. \qquad \text{(S2)}$$

Here κ(erg/cm s K) is thermal conductivity of DT, q is the heat released in one β-decay reaction, λ(1/s) is the frequency of β-decay, ω is specific molecular DT volume, H_s is the sublimation heat, and h is the layer thickness. Solution of the problem (S1), (S2) is:

$$V = \beta(T_e - T_0 - \lambda q h^2/4\omega\kappa)/(1 + \beta h H_s/\omega\kappa) \approx (\omega\kappa/hH_s)(T_e - T_0 - \lambda q h^2/4\omega\kappa). \qquad \text{(S3)}$$

The second equality uses estimates of kinetic coefficient β given in the next section. With this estimates, $\beta h H_s/\omega\kappa = 5.10^3 >> 1$ showing that solidification, or evaporation, or melting rate is overwhelmingly controlled by heat transport rather that by interface incorporation. Eq.(S3) also provides maximal layer thickness $h = [4\omega\kappa(T_e-T_0)/q\lambda]^{1/2} \sim$ 100mkm at $T_e-T_0 = 1$mK. Typical time necessary to make the layer thickness constant over the whole sphere at equilibrium follows from eq. (S3) at $T_e = T_0$, and is $\sim h/V = 4H_s/q\lambda \sim 1.8$ hour, vs experimental ~0.5 hour.

On the initial crystal segment emerging from the fill tube, the two opposite basal planes are exposed to the vapor and thus may be taken as thermally isolated. Thus the temperature at the rough crystal-vapor interface parallel to the capsule wall and looking towards the sphere center may be estimated as the temperature at the internal surface of spherical layer, as determined by eqs.(S1),(S2). Therefore the belt height, in agreement with observations, is automatically adjusted not far away from the final layer thickness from the very beginning. The two end surfaces of the initial segment are also rough but are in contact with the cold capsule wall and thus grow at highest velocity controlled by latent heat transport through the wall.

2. Kinetic coefficients, β(cm/s.K). For growth from vapor, we take sticking coefficient to be unity [9]. Then $\beta = \omega(\partial P_e/\partial T)/(2\pi mkT)^{1/2} = 6.5$cm/sK. For melt growth [L.V.Mikheev, A.A.Chernov, J.Crystal Growth, 112(1991)591-596; G.H.Rodway, J.D.Hunt, J.Cryst Growth 112(1991)] $\beta = 1.3(kT/m)^{1/2} H_f/kT^2 = 1.7.10^3$cm/sK, where $m = 8.35.10^{-24}$g and $\omega = 3.3.10^{-23}$cm^3 are the DT molecular mass and volume (in solid), T=19K, and latent heat of fusion $H_f = 3.62.10^{-15}$erg [9]. These βs justify the second approximate equality in eq.(S3). In other words, the growth rate, indeed, is controlled by release of the latent and β-decay heat to the capsule kept at the temperature T_0. Typical rate for this release is $\omega\kappa/ch \sim 0.1$cm/s strongly exceeding experimental $V \sim 10^{-5}$cm/s but is much less than the typical interface incorporation rate $\beta H_s/c$ or $\beta H_f/c$ [7] where $c = 2.9.10^{-16}$erg/K is the DT heat capacity per molecule.

3. Groove profile. The curved groove interface must be at phase equilibrium with the vapor. Thus the saturated vapor pressure over that curved interface (which is assumed to be isotropic) must be the same as over the flat interface away from the groove:

$$(1+(dy/dx)^2)^{-3/2}\ \omega\gamma d^2y/dx^2 - (H_s nq\lambda r_0/3\kappa T)y - (H_s q\lambda/2\omega T)y^2 = 0. \qquad \text{(S4)}$$

The first term presents increase of the chemical potential at crystal-vapor equilibrium due to the interface curvature. The second term is decrease of this potential due to decrease of temperature towards the wall due to β decay heat in vapor. The third term is similar decrease due to β decay in DT layer of thickness y and follows from eq.(S2) above, to the accuracy y^2. The vapor/solid density ratio, $n\omega \ll 1$, makes the second term comparable with the third only at y < 70nm. Therefore we truncate eq.(S4) to eq.(1) of the main text. In the metallurgical case [12], the groove profile that solves eq.(S4) is determined by the first and the second terms in eq.(S4) while in our case it comes from the first and the third terms. In the dimensionless coordinates, $\xi = x/\lambda, \eta = y/\lambda$, eq.(S4) has the integral:

$$\int_0^{\eta_0} \frac{(1-\eta^3/3)d\eta}{[1-(1-\eta^3/3)^2]^{1/2}} = |\xi|, \quad \eta_0 = 3^{1/3}[1-\frac{1}{(1+p_0)^{1/2}}]^{1/3}. \qquad \text{(S5)}$$

Integration at $\eta^3/3 \ll 1$ gives

$$(1+\eta^3/20)/\eta^{1/2} = (1+\eta_0^{\ 3}/20)/\eta_0^{\ 1/2} + |\xi|/6^{1/2}. \qquad \text{(S6)}$$

Ignoring terms cubic in η and η_0 in eq.(S6) we obtain eq.(2) of the main text.

4. Inhomogeneous grain. To influence the groove shape, shift of the chemical potential due to residual stress from not relaxed dislocation network should be compable with the increase Δμ of the DT chemical potential due to the temperature decrease near or below the cusp level, $y=y_0$, eq.(1). The temperature induced shift $\Delta\mu \sim cq\lambda H_s y_0^2/2\omega\kappa T = 5.10^{-21}$erg. The stress shift should be a small part of the elastic thermal stress energy, $E(\alpha\Delta T)^2\omega/2 = 6.10^{-19}$erg. The ratio of the former number to the latter is ~0.01. Thus, residual stress of a reasonable 1% could make equilibrium pressure shift due to inhomogeneity in the dislocation density distribution within a grain comparable with the shifts due to the temperature and curvature change along the groove balanced by eq.(1)..

5. Ripening rate. Near melting temperature, the creep rate is limited by point defect diffusion and dislocation glide [Modern Crystallography IV]. For an estimate in the DT single crystal layer with relatively big grains and low layer thickness, we ignore possible glide and diffusion along grain boundaries. Then the strain rate [13] may be taken as $d\varepsilon/dt = -14E\varepsilon\omega//kTh^2$ where Eε substitutes macroscopic stress driving the process and the empirical numerical factor 14 is used. Though E has the dimension of Young modulus it is hardly the real Young modulus as determined from speed of sound, $E_s = 5.10^9$ erg/cm^3.[6] Indeed, D_2 and H_2 in the cm-size polycrystalline samples show no elasticity for tensile strain down to at least $\varepsilon \sim 10^{-3}$ at temperatures 1.4 – 17K employed [6] since even linear experimental stress-strain dependence shows a plastic hysteresis. The apparent Young modulus, E, following from this linear dependence increases with number of tension cycles. Thus E should mean resistance to the tension of both the lattice and the dislocation network and depend on the strain rate. Therefore for the

ripening rate estimate given above it is more relevant to use apparent modulus $E = 3.10^8$ erg/cm3 [6], ~ 20 times lower than E_s.

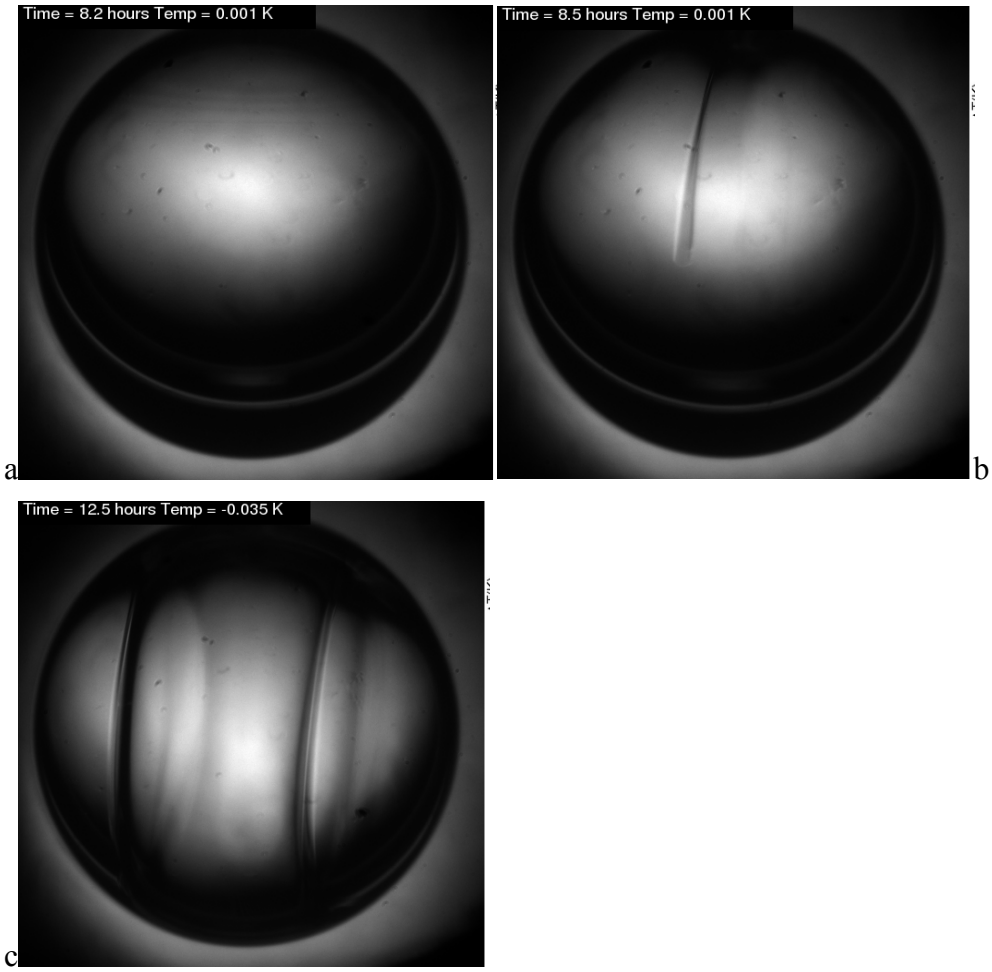
Time = 8.2 hours Temp = 0.001 K
a
Time = 8.5 hours Temp = 0.001 K
b
Time = 12.5 hours Temp = -0.035 K
c

Fig 1 a,b,c

Fig 2 a,b,c,d

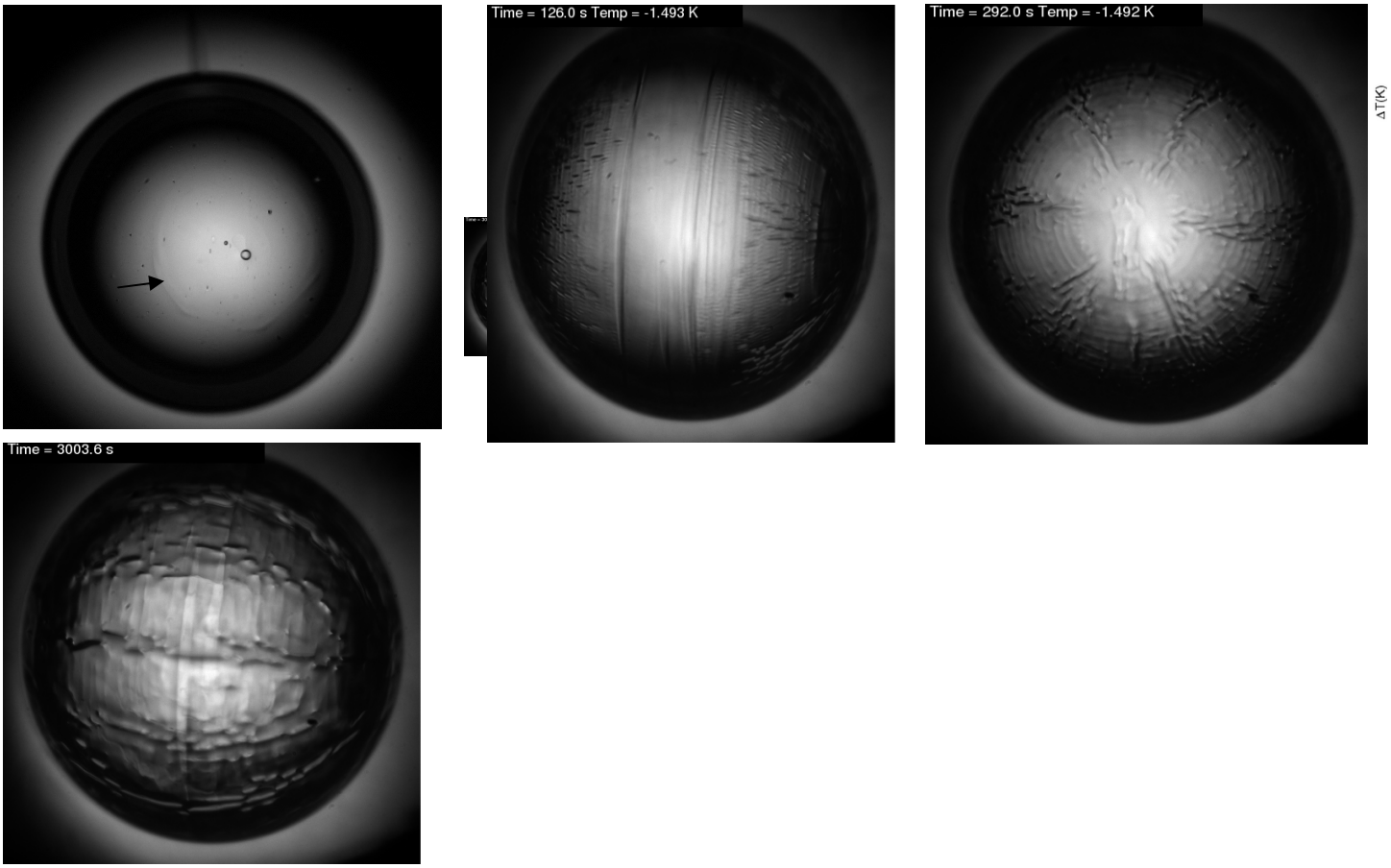

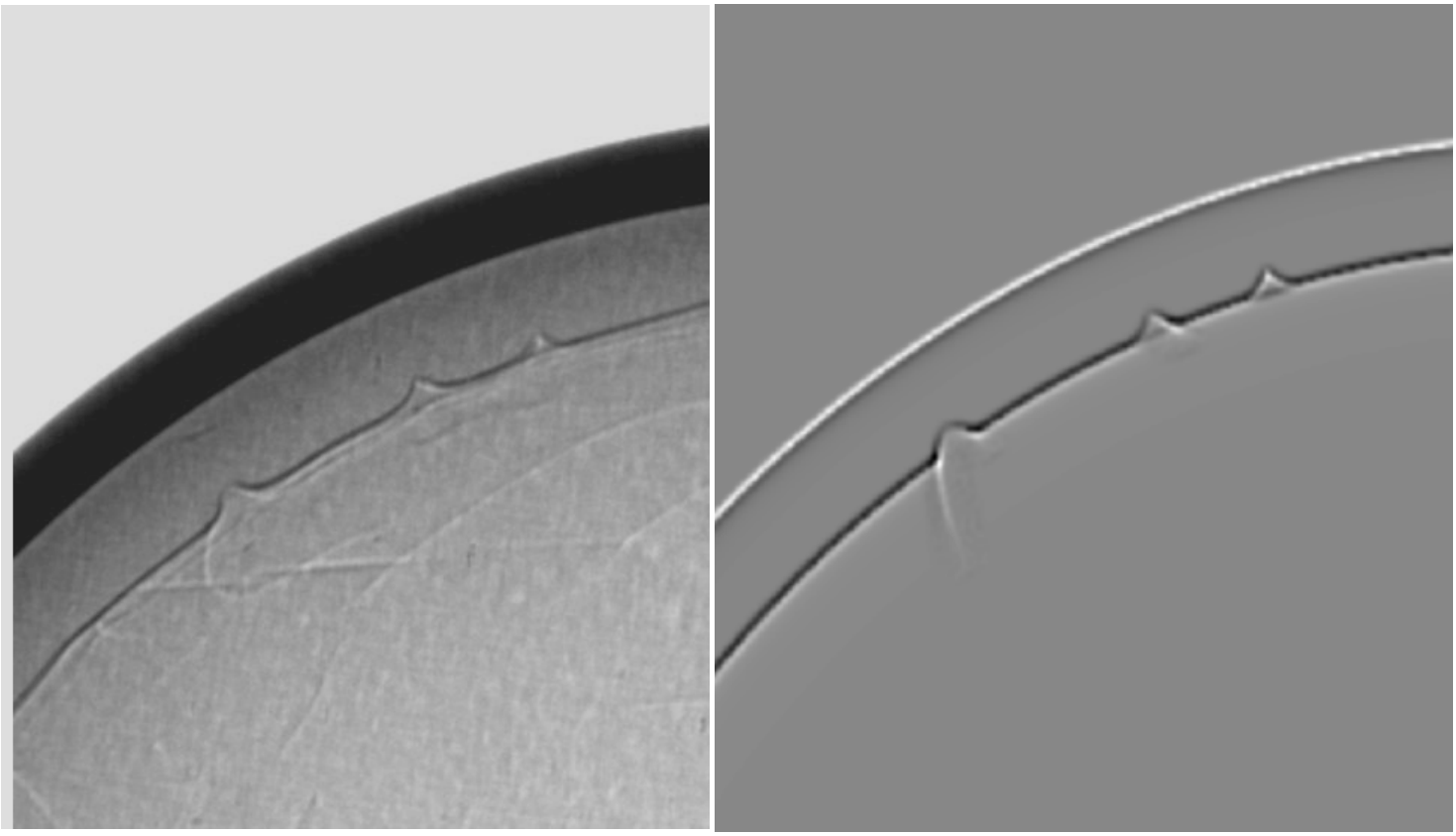

Fig 3 a, b

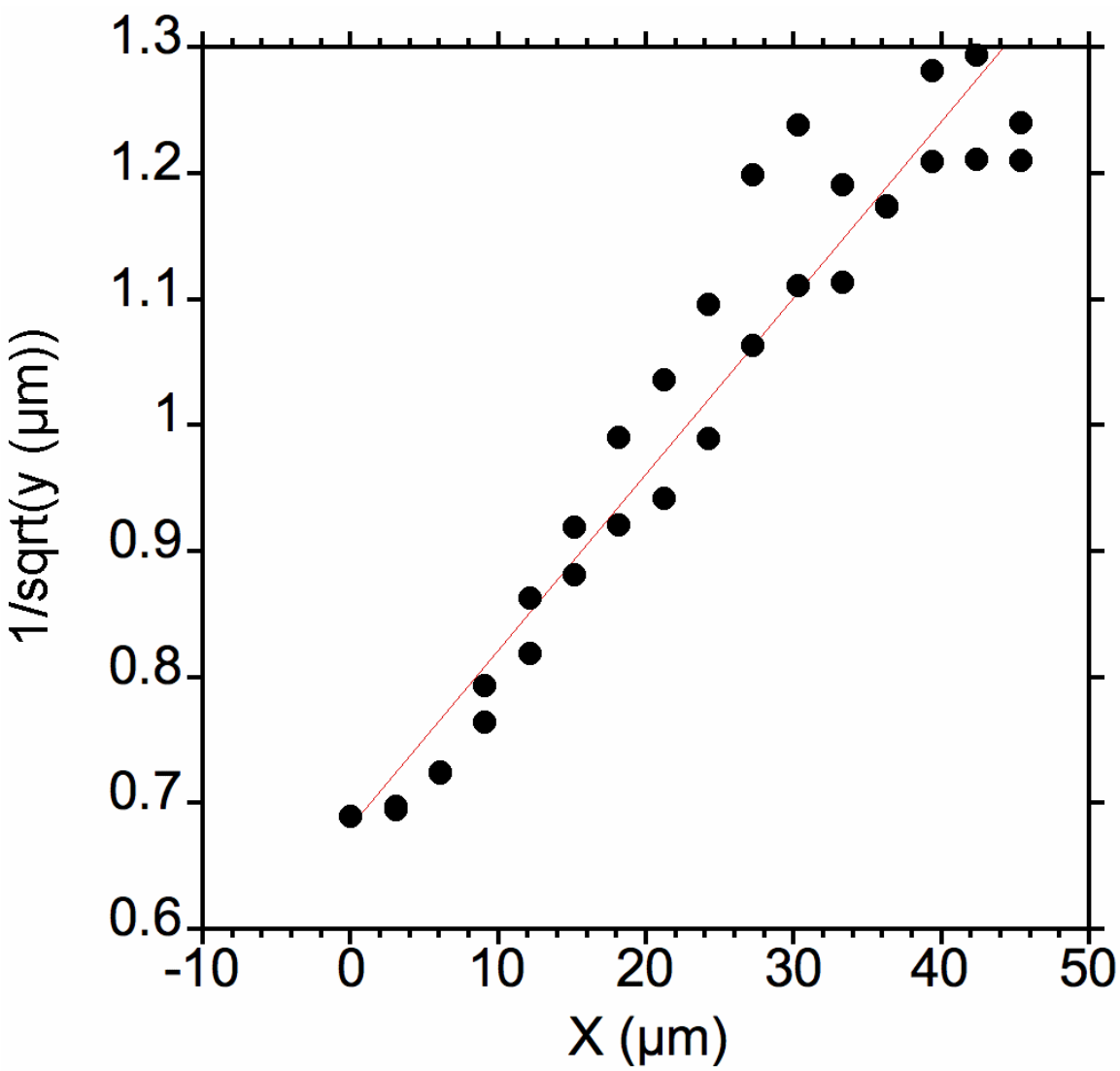

b